Applied Surface Science 493 (2019) 212–224

Contents lists available at ScienceDirect

Applied Surface Science

journal homepage: www.elsevier.com/locate/apsusc

Full length article

# Contact stiffness effects on nanoscale high-speed grinding: A molecular dynamics approach

Michail Papanikolaou*, Konstantinos Salonitis

*Manufacturing Theme, Cranfield University, Cranfield MK43 0AL, United Kingdom*

ARTICLE INFO

*Keywords:*
Nanoscale grinding
Contact stiffness
Real depth of cut
Molecular dynamics
Fractal roughness

ABSTRACT

One of the most important grinding parameters is the real depth of cut which is always lower than its programmed value. This is because in reality abrasive grains of the grinding wheel are not fixed but attached to a bonding material which is deformed during the process. In this study we investigate the effect of the contact stiffness between a single abrasive grain and the workpiece on the depth of cut and the grinding process characteristics via three-dimensional Molecular Dynamics (MD) simulations. Contact stiffness has been modelled by attaching a single trapezoid abrasive grain to a spring in the normal grinding direction. MD experiments have been repeated due to the stochastic nature of the grinding process in favour of statistical accuracy. Various grinding speeds have been considered while the case of a rough abrasive-workpiece interface has been investigated as well using fractal models. Our results indicate that the trajectory followed by the abrasive grain is not a straight line, as in the case of a rigid abrasive, but a curved one, asymptotically converging towards the equilibrium point which corresponds to the selected value of the spring stiffness. This behaviour alongside the grinding velocity and rough abrasive-workpiece interface have been found to affect the grinding forces, friction coefficient, morphology of the ground surface and subsurface temperature. The present MD model has also been proven to be capable of capturing the thermal softening phenomenon at the abrasive-workpiece interface.

## 1. Introduction

Grinding is one of the most interesting manufacturing processes in terms of numerical modelling due to its stochasticity and the multiscale phenomena involved. Stochasticity is mainly related to the random shape and size of the abrasive grains embodied, through the bonding material, in the grinding wheel as well as their geometrical distribution. Grinding has been numerically modelled in various scales ranging from nano- to continuum [1]. Nowadays, many researchers focus on understanding the fundamental phenomena taking place during the grinding process, such as the interaction between a single abrasive grain and the workpiece; thus, micro- and nanoscale investigations are in the spotlight. Although micro- and nanoscale simulations are computationally expensive, thanks to the rapid evolution of the computing power they are nowadays feasible. The interaction between a single abrasive grain and the workpiece has mainly been investigated via three numerical methods, namely Finite Element Analysis (FEA), Discrete-Element Modelling (DEM) and Molecular Dynamics (MD) [1]. MD simulations have often been utilised due to their capability to capture atomistic detail and offer a deeper understanding of micro- and nanoscale phenomena.

During the past years a number of studies have utilised MD to investigate the interaction between a single abrasive grain and the workpiece. The first MD studies on grinding were two dimensional and utilised conventional pair potentials such as the Lennard Jones (LJ) [2] and Morse [3] potentials to model the interaction between the workpiece and abrasive grain atoms. Those studies focused primarily on the estimation of the cutting forces as a function of the cutting depth, tool geometry, cutting speed and specific energy [4–6]. More recent studies utilised many-body potentials, such as the Embedded Atom Model (EAM), which account for the interaction between 3 or more particles [7]. Many-body potentials have been proven to offer increased accuracy compared to conventional interatomic ones, which can lead to the overestimation of the grinding forces [8]. Moreover, the latest MD investigations of grinding processes have been expanded to 3 dimensions instead of 2 and concerned with a variety of topics including (a) subsurface damage [9,10], (b) multi-grit grinding [11] and (c) surface roughness [12,13]. The shift from 2-dimesional simulations to 3-dimensional ones was because of the 3D nature of metal crystals; deeper insight is obtained with 3D simulations which enhance accuracy and provide a more realistic representation of the system [14,15].

An interesting topic that has not yet been thoroughly investigated in

* Corresponding author.
*E-mail address:* m.papanikolaou@cranfield.ac.uk (M. Papanikolaou).

https://doi.org/10.1016/j.apsusc.2019.07.022
Received 14 May 2019; Received in revised form 28 June 2019; Accepted 3 July 2019
Available online 04 July 2019

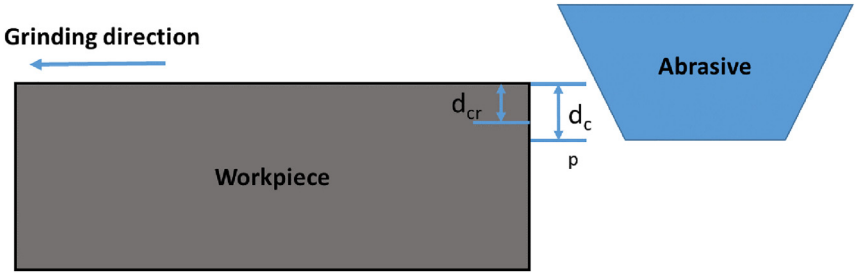


**Fig. 1.** Programmed vs. real depth of cut.

the atomistic level is the effect of the binder stiffness on the grinding process characteristics. Abrasive grains are not fixed but attached to their positions on the grinding wheel with the help of a binder, which is being deformed during the process. This is expected to affect the real depth of cut, which is defined as the thickness of the metal layer removed. The real depth of cut ($d_{cr}$) is always lower than its programmed value ($d_{cp}$) due to the displacement of the binder of the grinding wheel as well as the abrasive grains (Fig. 1). The first study to consider the elastic displacement of the abrasive grains during the grinding process was performed by Hahn [16]. Their model consisted of abrasive grains attached to individual springs. They attempted to identify the reason behind the increased removal rate when the difference between the wheel and the workpiece curvature is large while the magnitude of the grinding forces is kept constant. They suggested that, when the curvature difference between the workpiece and the wheel is large, there are more active grains per unit area of wheel surface due to the smaller deflection of the grains. This leads to increased removal rate. The concept of modelling the elastic displacement of the abrasive grains with the use of springs was adopted and modified by the latest Discrete-Element Modelling (DEM) techniques. More specifically, in DEM models, parallel bonds (also called beams in some studies) are used in order to connect the grains with the binder particles [17] as illustrated in Fig. 2. The coefficients characterising the stiffness of these bonds are calibrated against experimental results in order to realistically represent the mechanical properties of the grinding wheel. A very interesting DEM investigation was performed by Osa et al. [18] which accounted for the viscoplastic behaviour of the workpiece as a function of the strain rate and temperature according to the Johnson-Cook model [19]. Their DEM model was proven to be efficient in capturing the effects of grinding wheel surface topography, depth of cut and grain density on the contact length, which is defined as the largest distance of grains being in contact with the workpiece. Moreover, the effects of the grinding wheel topography and the dressing conditions on the contact area and wheel deformation were investigated. The only MD investigations focusing on the grinding wheel stiffness effects on the process characteristics have been performed by Shimizu et al. [23,24]. The authors performed 2-dimensional MD simulations to investigate the effects of the grinding wheel stiffness on the grinding process characteristics. However, their MD model is limited to two dimensions, simplified potentials have been used (Morse) instead of multibody ones, such as EAM, while the focus of this study has been laid on the grinding forces, depth of cut and the stick-slip motion of the abrasive.

Although DEM is based on the calculation of the particles' trajectories and the interactions between them, it should be classified as a mesoscale method [20]. More specifically, particles in DEM correspond to groups of atoms. The interaction parameters between the DEM particles are calibrated so as to reproduce either numerical or experimental results. Therefore, due to the fact that a significant amount of atomistic detail is averaged out, DEM is not suitable for studying nanoscale phenomena, such as the interaction of a single abrasive grain with the workpiece during nanoscale grinding. Moreover, nanoscale high speed grinding is a process that cannot be efficiently analysed via experiments due to the very small scales involved as well as the concurrent interaction of diverse phenomena such as subsurface damage, tool wear and strain rate [21]. In contrast to DEM and experiments, MD offers excellent spatial and temporal resolution, since the positions and momenta of the atoms contained in the simulation domain are calculated in each timestep. Moreover, the interactions between atoms are estimated using well established force fields and potentials [22].

The research focus of this investigation is laid on the interaction between a single abrasive grain and the workpiece. For the investigation of such small scale systems, a high level of accuracy with respect to the interaction potentials and particle resolution is required. Moreover, the employed model should be able to capture a number of nanoscale phenomena including the elastic recovery and heating of the workpiece, crack propagation, dislocation movement and microstructure alteration. With regard to the aforementioned phenomena, MD has a significant competitive advantage over DEM and experimental measurements as it can accurately analyse the interaction between the abrasive and the workpiece without the need to make any ab initio assumptions. Therefore, MD has been selected as the most favourable modelling technique.

Although previous MD investigations have covered a wide range of topics on high-speed grinding, there is still limited knowledge on the effects of contact stiffness on the grinding process characteristics such as grinding forces, friction coefficient, induced vibrations and

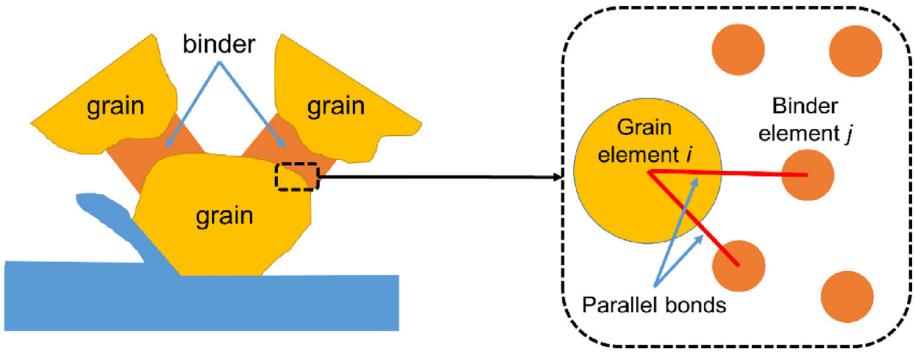


**Fig. 2.** Parallel bonds in DEM.

subsurface temperature. With the exception of the 2 dimensional models of Shimizu et al. [23,24], who performed 2 dimensional MD simulations and focused mostly on the grinding forces, the rest of the studies do not employ contact stiffness models and consider that the abrasive grain cannot move along the normal grinding direction; this is an oversimplification of the real process. The present study aims to address these knowledge gaps via 3 dimensional MD simulations. This investigation has also been expanded to the mutual interaction of contact stiffness with grinding speed and rough abrasive-workpiece interface (modelled using fractals) and study their combined effects on the aforementioned grinding process characteristics. The obtained results suggest that all of the parameters under investigation as well as their mutual interaction significantly affect the aforementioned process characteristics and are in agreement with previous experimental observations and numerical models. The elevated temperature observed in the vicinity of the abrasive grain is strongly linked to the thermal softening of the workpiece which has been effectively captured via MD simulations in the current investigation.

## 2. Simulation method

As illustrated in Fig. 3, the MD simulation setup consists of a diamond trapezoidal abrasive grain and a copper workpiece. The characteristic dimensions of the abrasive grain and workiece are listed in Table 1. The selection of the trapezoidal geometry was based on the fact that abrasive grains present a large negative rake angle [6]. Moreover, diamond and copper were selected as their corresponding bulk and interaction potentials have been well established in the literature. As illustrated in Fig. 3, there are 4 types of atoms in the simulation domain, namely (a) rigid, (b) thermostat, (c) Newtonian and (d) spring atoms. This simulation setup has also been implemented in previous MD simulations on nanoscale grinding [9,12,23]. Layers of rigid atoms were used to fix the position of the workpiece, which is clamped in reality. A Langevin thermostat [26] was applied to the thermostat atoms in order to control the temperature of the two solids, which was initially set equal to the ambient temperature (300 K). The thermostats were applied to the outermost layers of the two solids and had no effect on the dynamics of the Newtonian atoms, which gradually acquired the desired temperature during the equilibration stage. The spring atoms were tethered to their initial positions, which corresponded to the diamond lattice sites as it will be explained in the following paragraphs. The spring force was applied to the y axis direction (normal grinding direction) in order to model the elastic behaviour of the abrasive grain due to the deformation of the binder. It has to be mentioned that in many MD investigations the abrasive (diamond) atoms are considered to be immobile [25]. Although this approach might yield accurate results, it neither allows for the temperature control of the abrasive nor realistically emulates the dynamics of the system. Finally, the trajectories of Newtonian atoms were estimated by integrating the classical Newton's equations of motion.

**Table 1**
Characteristic dimensions.

| | | |
|---|---|---|
| Workpiece | Length (x) | 900 Å |
| | Height (y) | 54 Å |
| | Width (z) | 159 Å |
| Abrasive | Upper edge (x) | 195 Å |
| | Lower edge (x) | 79 Å |
| | Height (y) | 79 Å |
| | Width (z) | 9 Å |

The lattice structure as well as the interaction potentials for the two materials considered have been well established in the literature [27]. The workpiece copper atoms and the grain diamond atoms are placed on the sites of a FCC lattice with a lattice constant equal to 3.597 Å and a diamond lattice with a lattice constant equal to 3.57 Å respectively. The [100] direction on the (001) plane of the FCC lattice of the copper workpiece is parallel to the x axis, which coincides with the grinding direction.

Three different potentials have been utilised to describe the interactions between the simulation atoms. The interaction between the copper atoms (Cu−Cu) was modelled via the many-body EAM potential, which has been developed by Daw and Baskes [7] and proven to be accurate and efficient for modelling metals [28]. According to the EAM potential, the total energy of a system consisted of $N$ atoms can be described by:

$$E_{tot} = \sum_{i=1}^{N} \left[ F_i(\rho_{h,i}) + \frac{1}{2} \sum_{j,j \neq i} \varphi_{ij}(\rho_{ij}) \right] \quad (1)$$

where $F_i$ is the energy required to embed atom $i$ in its current position, $\rho_{h,\,i}$ the local electron density and $\varphi_{ij}$ the repulsion between the atoms $i$ and $j$. The EAM potential allows for the deformation of the workpiece which is not considered to be immobile but stiff and deformable. The interaction between the diamond atoms (C−C) has been modelled using the Tersoff potential [29] which has been widely used for describing covalently bound clusters of atoms [30]. The total energy according to

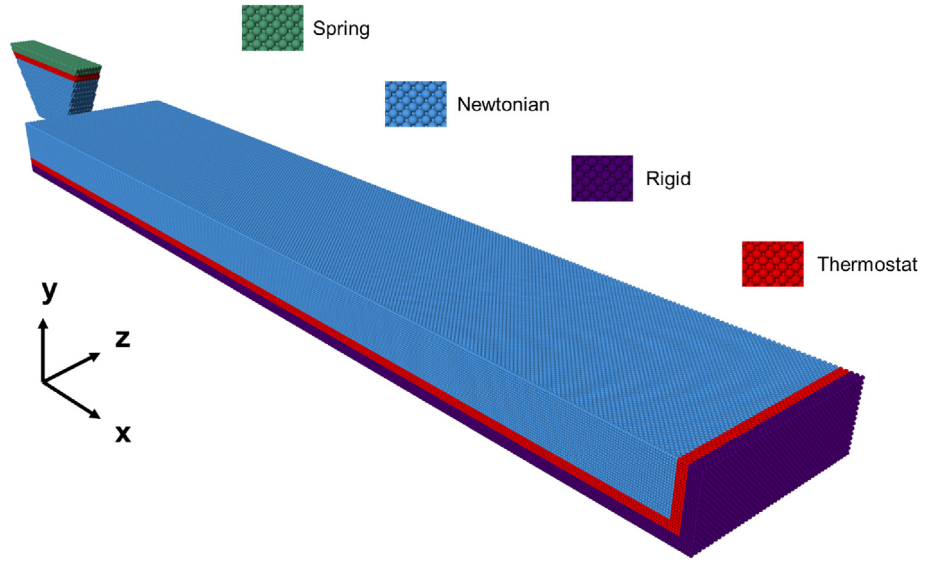


**Fig. 3.** Atom types in the simulation domain.

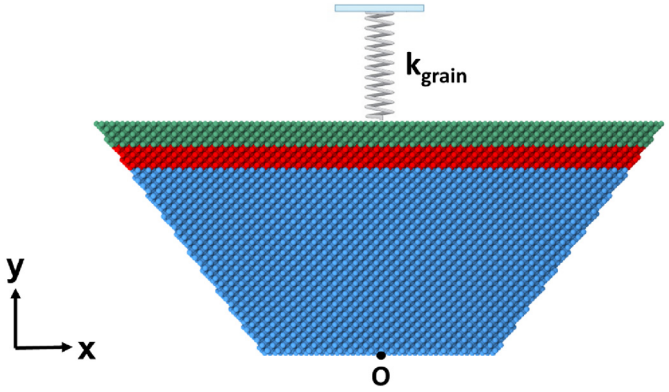


**Fig. 4.** Resultant spring constant.

the empirical Tersoff potential is given by:

$$E_{tot} = \sum_{j,j\neq i} f_c(r_{ij})[f_R(r_{ij}) + b_{ij}f_A(r_{ij})]$$

$$f_c(r_{ij}) = \begin{cases} 1 r_{ij} < R - D, \frac{1}{2} - \frac{1}{2}\sin\left(\frac{\pi}{2}\right)\frac{r_{ij} - R}{D} R - D < r_{ij} < R + D, 0 r_{ij} \\ > R + D \end{cases} \quad (2)$$

where $f_R(r_{ij})$ and $f_A(r_{ij})$ are the repulsive and attractive terms respectively, $f_c(r_{ij})$ the cutoff function which limits the potential forces within a specific distance range $[R - D, R + D]$ and $R$, $D$ constants selected so as to include only the first neighbouring cell. The potential energy between the copper and carbon atoms was modelled via the Morse potential [31] as defined in Eq. (3). In Eq. (3) $D_0 = 0.087\ eV$ is the cohesion energy, $a = 5.14$ the elastic modulus and $r_0 = 2.05\ \AA$ the equilibrium distance [32].

$$V(r_{ij}) = D_0[e^{-2a(r-r_0)} - 2e^{-a(r-r_0)}] \quad (3)$$

As mentioned in the Introduction section, the green atoms (Fig. 4) have been attached to springs with their spring force being applied only to the y direction. The spring force was not applied to the other 2 directions in order to eliminate stochasticity. The tangential ($F_x$) forces could only be affected by the stick slip phenomenon which is not expected to be dominant in such high grinding speeds and for relatively high values of the depth of cut. Moreover, the transverse forces ($F_z$) tend to fluctuate around zero due to symmetry. These springs attach each one of these atoms to their initial position and are parallel to each other. Therefore, the resultant spring constant of the grain (Fig. 4) is equal to the sum of the individual spring constants $k_i$ as follows:

$$k_g = \sum_{i=1}^{N_s} k_i \quad (4)$$

where $N_s$ is the total number of the spring atoms (Table 3). At this point it should be clarified that the term "grain stiffness", used throughout the text, refers to the elasticity exhibited by the binder of the grinding wheel and not to the grain material (diamond).

**Table 2**
W-M function parameters.

| | |
|---|---|
| $L_{MAX}$ (Å) | 60 |
| $L_{MIN}$ (Å) | 5 |
| M | 10 |
| C (Å) | 0.7 |
| $D_s$ | 2.0 |
| γ | 1.5 |

As pointed out by previous research studies the grinding characteristics have been proven to be dependent on the interface condition between the two solids (abrasive grain and workpiece) and not on the surface roughness of the workpiece top surface [12]. A wide variety of approaches have been applied in order to model surface roughness in nanoscale. The primitive ones utilised periodic patterns, such as rectangular [33], sinusoidal [34] and triangular [35] protrusions. However, the nature of surface roughness is far from this description; on the contrary, it is characterised by stochasticity and possesses multiscale features [36]. With respect to contact mechanics, one of the most realistic models for representing surface roughness is fractal geometry. The fractal approach has been found to be capable of predicting surface phenomena in a range of scales based on an observation at a particular scale [37]. The rough surface profiles of Fig. 5 were generated with the help of the multivariate Weierstrass Mandelbrot (W-M) function (as described in [38]), which has been widely used to model fractal surfaces. Three random phase matrices $\Phi$ have been used for generating random surfaces while the corresponding W-M parameters are listed in Table 2. In order to investigate the contact stiffness effects in the case of a rough abrasive-workpiece interface we introduced rough surface profiles at the bottom face of the trapezoidal abrasive as illustrated in Fig. 5.

Before the abrasive starts moving, energy minimisation is performed until the local potential energy minimum of the system has been reached. Energy minimisation is followed by an equilibration stage, conducted under the NVE ensemble (constant number of atoms $N$, system volume $V$ and energy $E$), for 30,000 timesteps. By the end of the equilibration stage the temperature and pressure of the system have obtained constant values. Subsequently, a constant speed across the x direction is assigned to the spring atoms of the grain, initiating the grinding process. It has to be mentioned that the x velocity imposed on the spring atoms does not affect the dynamics of the system since the spring force is applied solely on the y direction. The simulation parameters are summarised in Table 3. The MD simulations were performed on 16 cores, with a simulation time equal to 48 h, using the LAMMPS molecular dynamics simulator [39,40].

Our simulations have been performed for 3 values of the grinding speed: (a) 100 m/s, (b) 200 m/s and (c) 300 m/s; furthermore, an additional case with a grinding speed equal to 100 m/s and a rough abrasive-workpiece interface was investigated. For each one of these

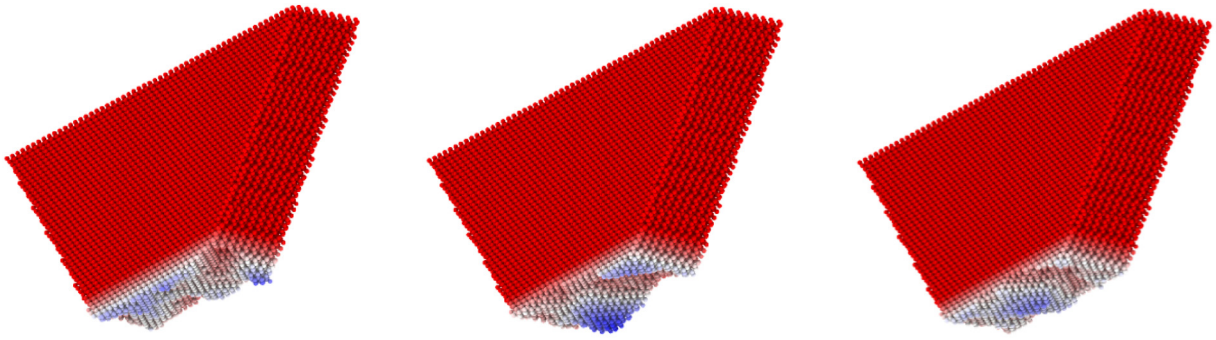

**Fig. 5.** Rough surface profiles of the abrasive bottom face.

**Table 3**
Simulation parameters.

| | |
|---|---|
| Total number of atoms | 754,805 |
| Initial temperature (K) | 300 |
| Programmed depth of cut $d_{cp}$ (nm) | 3 |
| Number of spring atoms $N_s$ | 4,482 |
| Timestep $t_s$ (fs) | 1 |
| C-mass (amu) | 12.011 |
| Cu-mass (amu) | 63.546 |
| Individual spring stiffness $k_i$ (nN/Å) | 0.002, 0.004, 0.008, 0.016 and 0.032 |

**Table 4**
Experimental design.

| Grinding speed $v_g$ (m/s) | Interface type | Grain stiffness $k_g = N_s \cdot k_i$ (nN/Å) |
|---|---|---|
| 100 | Smooth | 8.98 |
| | | 17.95 |
| | | 35.90 |
| | | 71.81 |
| | | 143.62 |
| 200 | Smooth | 8.98 |
| | | 17.95 |
| | | 35.90 |
| | | 71.81 |
| | | 143.62 |
| 300 | Smooth | 8.98 |
| | | 17.95 |
| | | 35.90 |
| | | 71.81 |
| | | 143.62 |
| 100 | Rough | 8.98 |
| | | 17.95 |
| | | 35.90 |
| | | 71.81 |
| | | 143.62 |

cases, 5 values of the grain spring constant have been considered (Table 4). Each simulation case was performed 3 times with a random seed value (initial distribution of atoms' velocities) to improve statistical accuracy and thus, 60 simulations were performed in total.

## 3. Results & discussion

In this section the effects of (a) contact stiffness, (b) grinding speed and (c) rough abrasive-workpiece interface on the grinding process characteristics (real depth of cut, grinding forces, temperature and friction coefficient) will be discussed. It will be shown that the real depth of cut is always smaller than its programmed value and this consequently affects the dimensional accuracy of the process. The obtained results suggest that all of the parameters under examination, as well as their combination, affect the grinding characteristics and performance. An overview of the morphology of the ground surface at 3 equally spaced timesteps ($N_{ts}$) is illustrated in Fig. 6.

### 3.1. Contact stiffness

As stated in the Introduction, the position of the abrasive grains of the grinding wheel is not fixed in reality; on the contrary, they are elastically displaced during the grinding process. The results presented in this subsection correspond to a grinding speed $v_g$ equal to 100 m/s. As illustrated in Fig. 7(a), for all cases examined, the tangential forces ($F_x$) increase with time. This is because of the continuous piling-up of material at the front of the abrasive grain. Moreover, it is evident that $F_x$ is affected by the grain stiffness which in this investigation is being controlled via the spring constant $k_g$; stiffer grains lead to increased $F_x$. Similar observations can be made for the normal forces ($F_y$) as illustrated in Fig. 7(b) although it appears that the effect of the grain spring constant on $F_y$ is not as dominant. A significant difference between Fig. 7(a) and Fig. 7(b) is that $F_y$ acquires an approximately constant value after the timestep $N_{ts}$ = 150,000. Thus, it can be concluded that in contrast to $F_y$, $F_x$ is affected by the material piling-up at the grain front. Moreover, it can be observed that $F_x$ asymptotically reaches a constant value, especially after the timestep $N_{ts}$ = 600,000. This is because the material piles at the grain front gradually acquire a constant size as the material piled up at the wake of the cutting region increases (Fig. 6).

Although Fig. 7 provides significant information about the dependence of the grinding forces on the grain spring constant, safer conclusions can be drawn if the simulations are repeated in favour of statistical accuracy. In Fig. 8 the average grinding forces over the timestep range 400,000 < $N_{ts}$ < 800,000, corresponding to 3 different MD experiments (with identical parameters but random seed), have been averaged and plotted against the spring constant along with the corresponding errorbars. It can be seen that both $F_x$ and $F_y$ reach asymptotically a constant value as $k_g$ increases. However, it appears that $F_y$ reaches this asymptotic value faster than $F_x$. This is attributed to the fact that $F_y$ is not affected by the chip piling up at the front of the grain in contrast to $F_x$.

In order to explain this behaviour the real depth of cut $d_{cr}$ was initially plotted as a function of time for the corresponding values of the grain spring constant (Fig. 9). As expected, the depth of cut is equal to the programmed value up to the point in time when the grain comes in contact with the workpiece. After this point, the real depth of cut gradually deviates from its programmed value; the lower the spring constant the higher the deviation. For low values of the grain spring constant ($k_g$ = *8.98 nN/Å*) the real depth of cut can reach values about 50% lower than the desired one (*30 Å*). Moreover, it can be observed that the grain stiffness affects the time required for the real depth of cut to reach a constant value; stiffer grains reach their real depth of cut faster than softer ones as illustrated in Fig. 9. This is because softer grains are displaced by a longer distance compared to the stiffer ones and thus, additional time is required until they reach their equilibrium point.

Similarly to the grinding forces, the real depth of cut (averaged over the range *400,000 < $N_{ts}$ < 800,000*) was averaged over 3 different

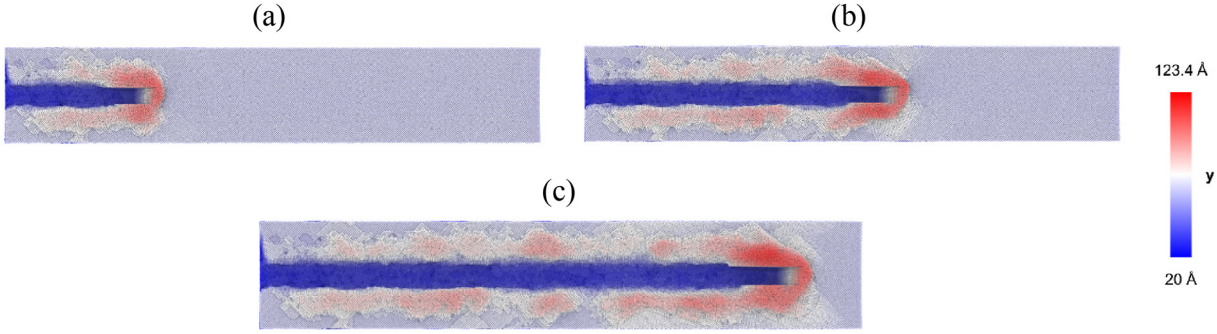


**Fig. 6.** Morphology of the ground surface at (a) $N_{ts}$ = 280,000, (b) $N_{ts}$ = 560,000 and (c) $N_{ts}$ = 840,000 ($v_g$ = 100 m/s, $k_g$ = 8.98 nN/Å).

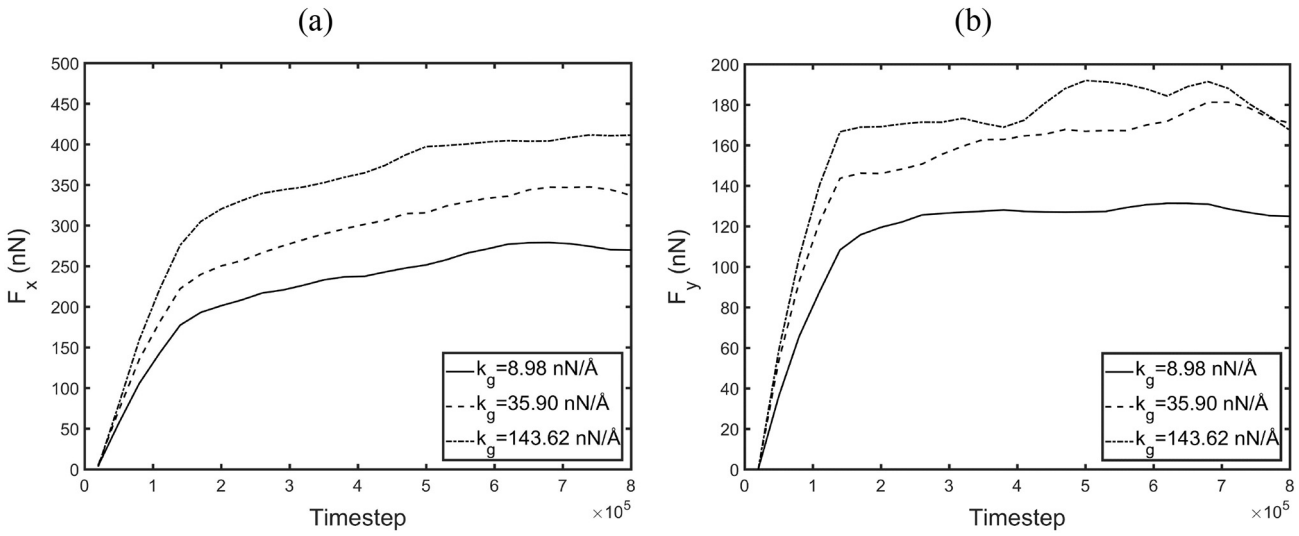


**Fig. 7.** (a) Tangential and (b) normal forces vs. time as a function of the grain spring constant.

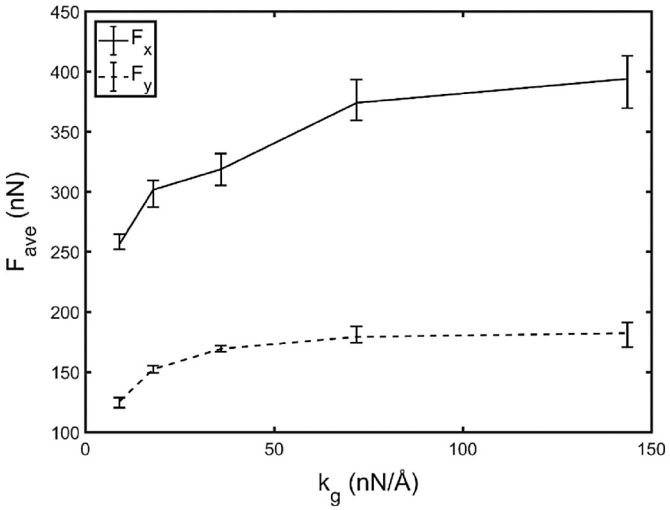


**Fig. 8.** Average grinding forces vs spring constant.

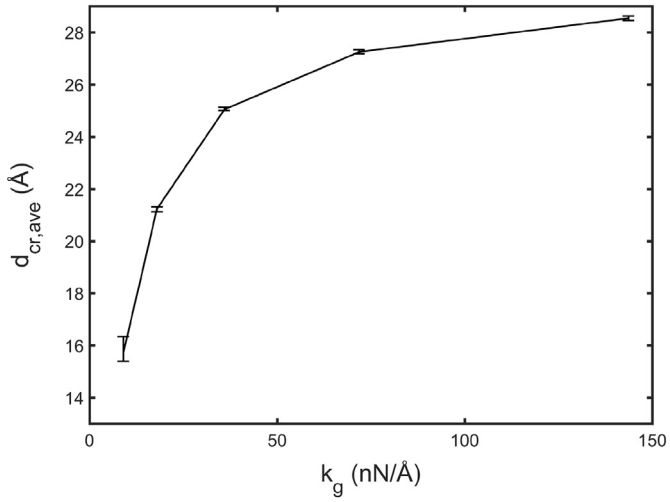


**Fig. 10.** Average depth of cut vs spring constant.

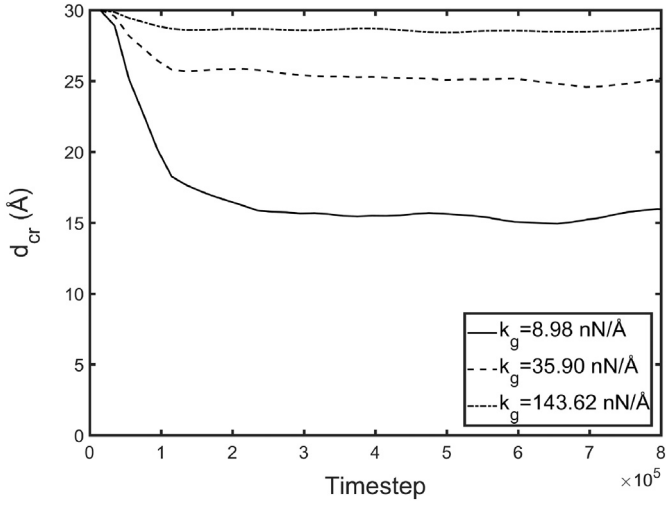


**Fig. 9.** Real depth of cut vs. time as a function of the grain spring constant.

simulations with different seed and plotted as a function of the grain spring constant. In Fig. 10 it can be observed that the average depth of cut increases asymptotically to its programmed value for higher values of the grain spring stiffness. Therefore, the increase of the grinding forces for higher values of the spring stiffness (Fig. 8) is attributed to the higher depth of cut [41].

Two additional observations that can be made are that (a) smoother depth of cut vs time curves (Fig. 9) and (b) lower errorbars (Fig. 10) are associated with higher values of the grain spring constant $k_g$. In order to investigate the vibration transmission for various values of the grain stiffness, the mean standard deviation ($STD_{ave}$) of the y coordinate of the grain centre of mass ($y_{com}$) was evaluated for each case ($400{,}000 < N_{ts} < 800{,}000$) and averaged over 3 simulations with different seed. From Fig. 11 it is clear that the average standard deviation drops with the grain spring constant. Therefore, it can be concluded that the higher the grain stiffness the lower the grinding tolerances.

Another important aspect of the grinding process is the temperature distribution over the workpiece, as the developed subsurface temperature profile during the process affects the final properties of the ground surface [42]. From the perspective of this investigation which focuses on the interaction of a single abrasive grain with the workpiece, it is of significant importance to measure the workpiece temperature at

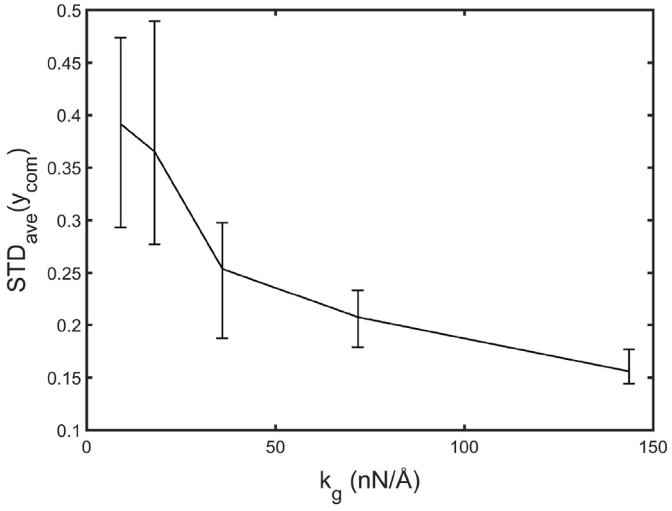


**Fig. 11.** Standard deviation of the y-coordinate of the centre of mass vs spring constant.

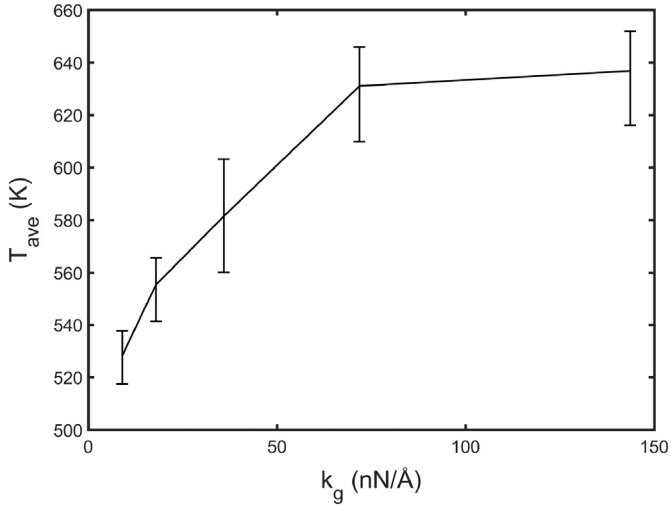


**Fig. 13.** Subsurface temperature vs spring constant.

the vicinity of the abrasive grain. Therefore, a spherical region with a radius equal to 10 Å was assumed and attached to the point O, as illustrated in Fig. 4. The workpiece atoms in this region were updated every 1 timestep and their temperature was evaluated as follows:

$$T = \frac{KE}{\frac{dim}{2} N k_B}$$

$$KE = \sum_{i=1}^{N} \frac{1}{2} m_i v_{z,i}^2 \quad (5)$$

where $KE$ is the kinetic energy, $dim = 1$ the number of the velocity components contributing to the evaluation of the $KE$ term, $N$ the total number of atoms lying within the sphere at the specific timestep and $k_B = 1.38 \cdot 10^{-23}\, m^2\, kg\, s^{-2}\, K^{-1}$ the Boltzmann constant. For the evaluation of the temperature only the z component of the atoms' velocities ($v_z$) has been considered since both $v_x$ and $v_y$ are affected by the grain and the chip velocity respectively and cannot provide an accurate estimate of the subsurface temperature. The temperature values were averaged over a time window of 2000 timesteps in order to eliminate the noise. As shown in Fig. 12, the workpiece subsurface temperature in the vicinity of the abrasive grain is slightly increasing during the evolution of the process. This is because of the fact that $F_x$ follows the exact same trend. Moreover, higher temperatures are observed for stiffer grains. This is attributed to the higher depth of cut which in turn leads to increased grinding forces as well.

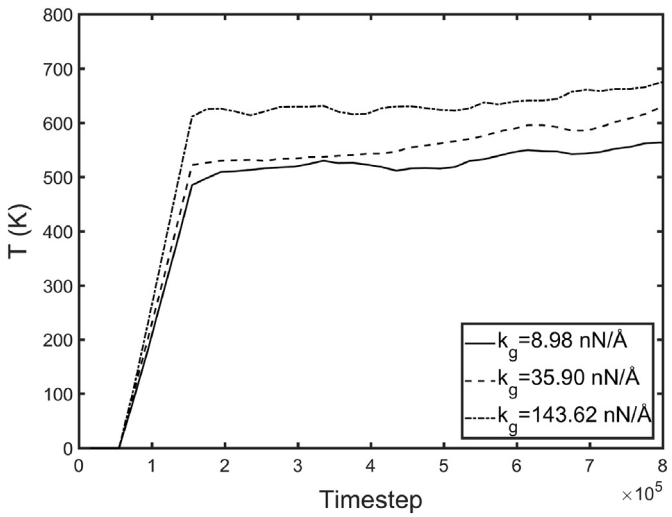


**Fig. 12.** Subsurface temperature vs. time as a function of the grain spring constant.

The dependence of the temperature on the grinding stiffness is more clearly illustrated in Fig. 13 where the average temperature over a timestep range has been averaged over 3 simulations with random seed and plotted against the grain spring constant with the corresponding errorbars. As expected, the trend of the temperature dependence on the grain stiffness is very similar to the one corresponding to the grinding forces (Fig. 8); higher grinding forces lead to increased heat dissipation.

In favour of greater understanding, 3 dimensional temperature profiles are presented in Fig. 14 ($N_{ts} = 400{,}000$). In order to obtain an enhanced view of the subsurface temperature, only half of the workpiece atoms are represented; a cross section at the half of the workpiece width ($z = w/2$) was used. Moreover, the abrasive grain atoms are hidden for enhanced clarity. The temperature of each atom depicted was estimated using Eq. (5) and averaged over a time window of 2000 timesteps to eliminate noise. Fig. 14 clearly shows that the hottest region of the simulation domain is located at the vicinity of the abrasive grain. Elevated temperature can also be detected at the ground surface which cools down gradually due the application of the Langevin thermostat. The temperature of the workpiece surface that has not been ground yet is equal to the initial temperature (300 K). Finally, the temperature of the atoms located at the bottom FCC layers is equal to 0 K as they are rigid and do not get time integrated. By comparing the two figures it can be observed that the temperature of the ground surface in Fig. 14(b), which corresponds to the stiffer grain, is much higher than in Fig. 14(a). Additionally, it is obvious that the depth of cut is higher when the grain is stiffer. Both of these observations are in accordance with the results presented in the previous paragraphs.

### 3.2. Grinding speed

In this subsection the combined effects of the grinding speed and contact stiffness on the grinding characteristics will be discussed.

The $F_x$ values have been plotted as a function of the grain spring constant for various values of the grinding speed in Fig. 15. $F_y$ appears to increase for higher values of the grain spring constant for all cases. This is attributed to the increase of the depth of cut, as discussed in Subsection 3.1. Moreover, it is clear that as the grinding speed increases, the grinding forces slightly reduce until they obtain a constant value. This trend is in agreement with previous MD investigations which suggest that when the grinding speed exceeds a threshold, $F_x$ remains constant [27] or is even reduced [10]. Similar observations were made by Anderson et al. [43] who performed both numerical and

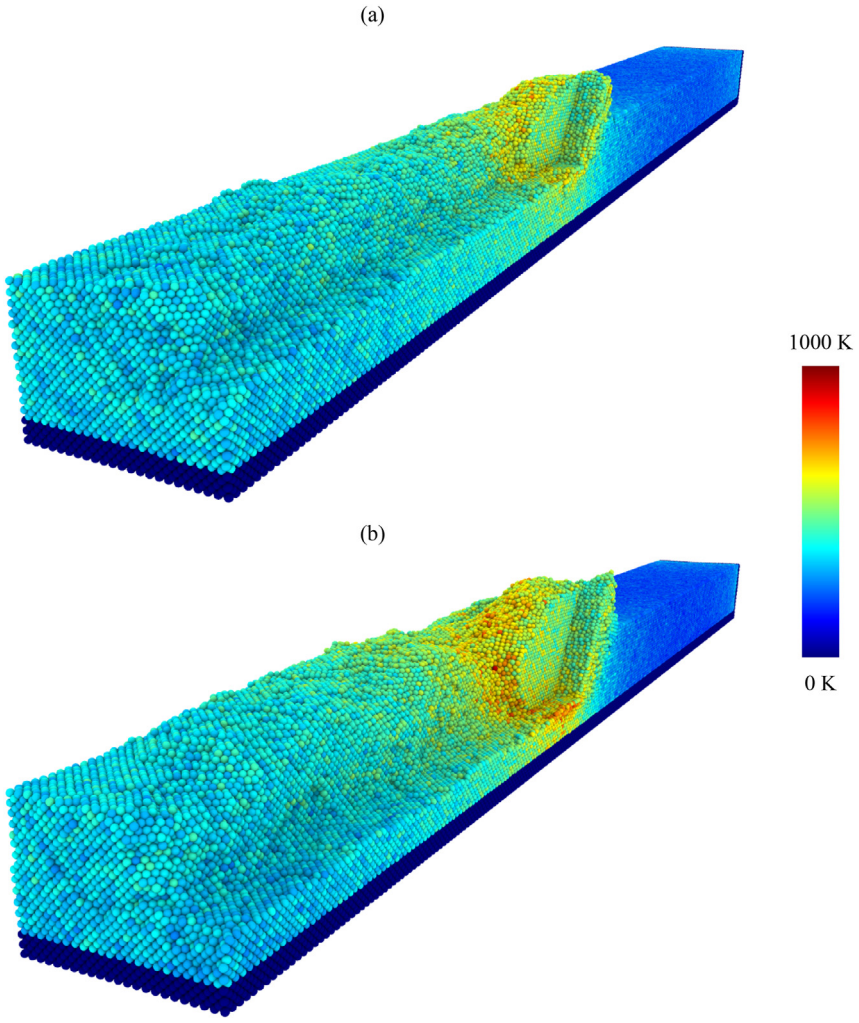


**Fig. 14.** Workpiece temperature for (a) $k_g$ = 0.00125 nN/Å and (b) $k_g$ = 0.02 nN/Å at $N_{ts}$ = 400,000.

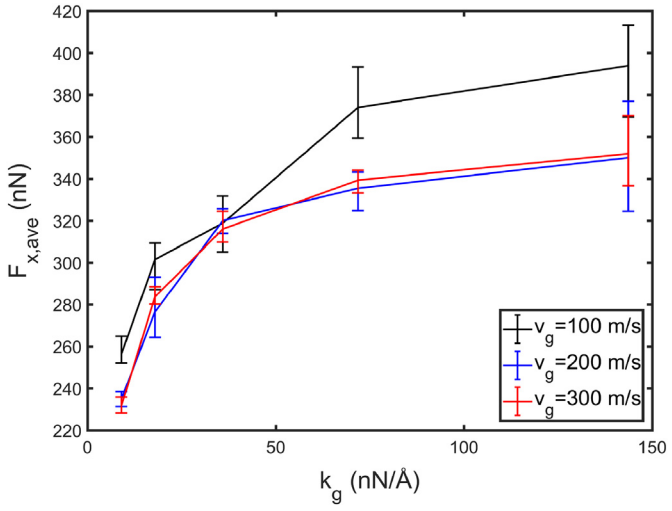


**Fig. 15.** Average tangential forces vs spring constant for various values of the grinding speed.

experimental investigations of single abrasive grain cutting and suggested that $F_x$ asymptotically decreases for higher grinding speeds due to a reduction in the friction coefficient. The decrease of $F_x$ for higher cutting speeds is attributed to the high temperatures and the consequent thermal softening of the workpiece [44,45].

On the other hand, $F_y$ appears to increase with the grinding speed. This is also in agreement with previous numerical and experimental studies [43] and is attributed to the increase of springback with strain rate as reported by Johnson and Cook [19]. Moreover, it can be seen that for high grinding speeds $F_y$ slightly decreases with increasing grain spring constant. This is because two phenomena with opposite effects are taking place at the same time: (a) stiffer grains lead to increased depth of cut and consequently higher $F_y$ and (b) stiffer grains also lead to higher temperatures (as it will be shown in the next paragraphs) which soften the workpiece and decrease $F_y$. As a result, $F_y$ tends to decrease after a threshold in the spring constant value has been exceeded; this behaviour is intensified for higher grinding speeds due to the higher subsurface temperature.

Previous numerical and experimental investigations have reported that the friction coefficient $\eta = F_x/F_y$ decreases with the grinding speed [43,44]. The current MD model yields similar results as shown in Fig. 17. Moreover, the friction coefficient appears to increase, non-monotonically though, with the grain spring constant. At this point, it has to be mentioned that the friction coefficient is larger than 1 which is not common in experiments. However, this behaviour appears to be common among various MD studies and is attributed to the chip formation force being more dominant in such small scales [41,46,47]. The value of the friction coefficient highly depends on a number of factors with the most important being the geometry of the abrasive grain and the hardness of the workpiece material.

As shown in Fig. 18, the depth of cut increases asymptotically with

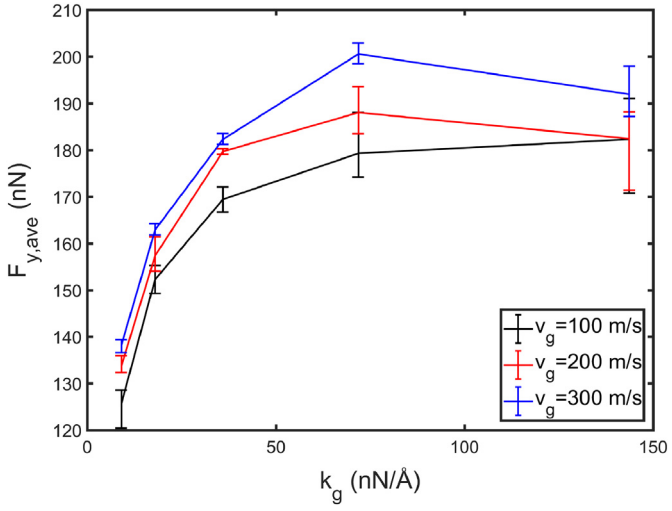


**Fig. 16.** Average normal forces vs spring constant for various values of the grinding speed.

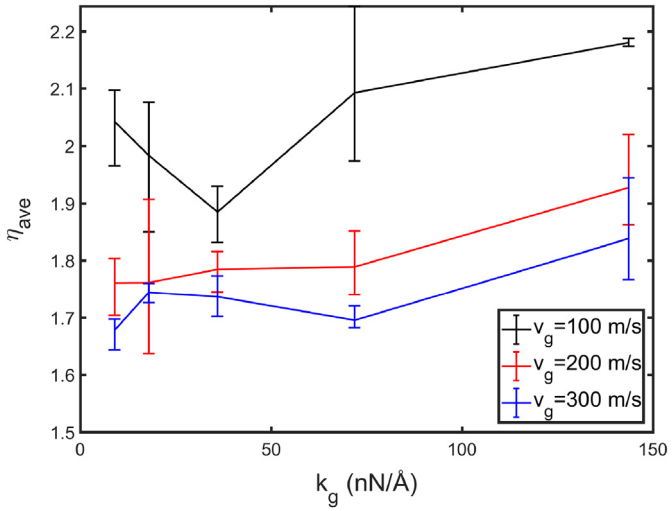


**Fig. 17.** Average friction coefficient vs spring constant for various values of the grinding speed.

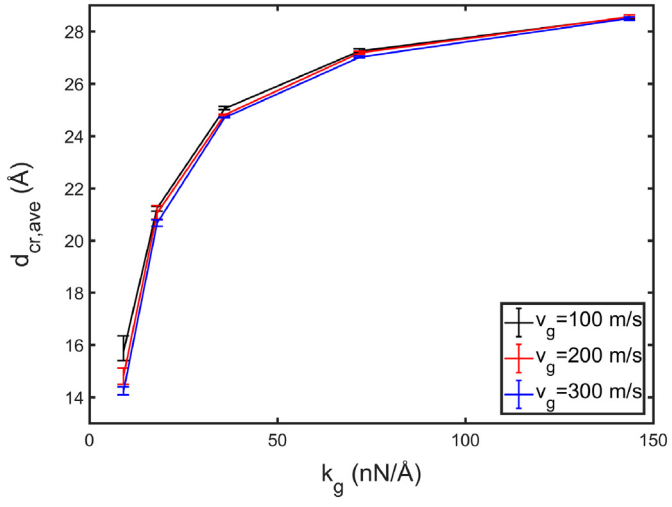


**Fig. 18.** Average real depth of cut vs spring constant for various values of the grinding speed.

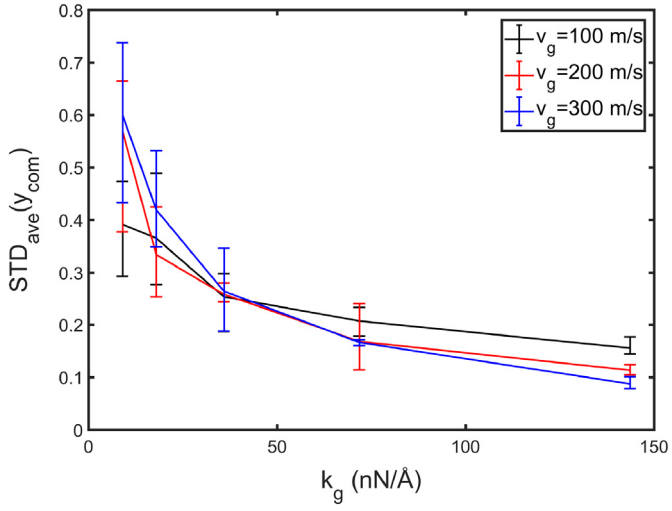


**Fig. 19.** Average STD of the y-coordinate of the centre of mass vs spring constant for various values of the grinding speed.

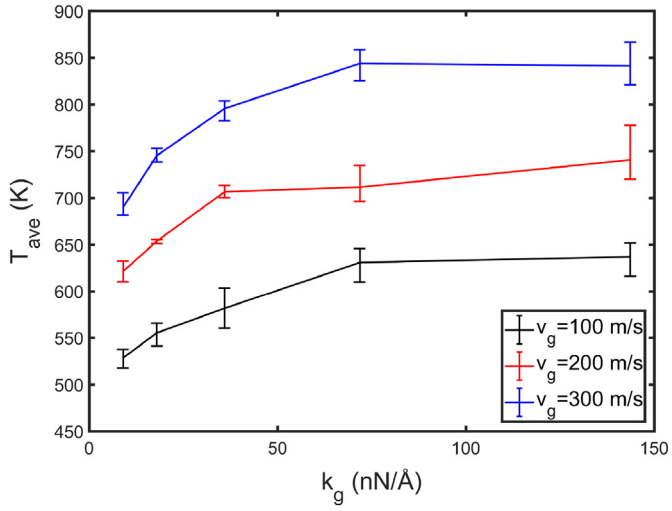


**Fig. 20.** Subsurface temperature vs spring constant for various values of the grinding speed.

the spring constant for all cases. Moreover, the depth of cut increasingly deviates from its programmed value for higher grinding speeds. However, this deviation is reduced as the spring constant $k_g$ increases. This behaviour can be interpreted by observing Fig. 16. Average normal forces ($F_{y,ave}$) obtain larger values for higher grinding speeds; this indicates that the abrasive grain increasingly deviates from its equilibrium point $y_e$ which can be defined as follows:

$$y_e = \frac{2 \bullet F_{y,ave}}{k_g} \tag{6}$$

With the help of Eq. (6), the real depth of cut $d_{cr}$ can be calculated as follows:

$$d_{cr} = d_{cp} - y_e = d_{cp} - \frac{2 \bullet F_{y,ave}}{k_g} \tag{7}$$

where $d_{cp}$ the programmed depth of cut. As shown in Fig. 16, $F_{y,ave}$ increases asymptotically with $k$. Thus the term $\frac{2 \bullet F_{y,ave}}{k_g}$ is about equal for all the values of the grinding speed and minor differences can be observed for large $k_g$ values. Consequently, as $k_g$ increases the values of the real depth of cut corresponding to various grinding speeds become gradually equal between them.

In order to investigate the quality of the ground surface the standard

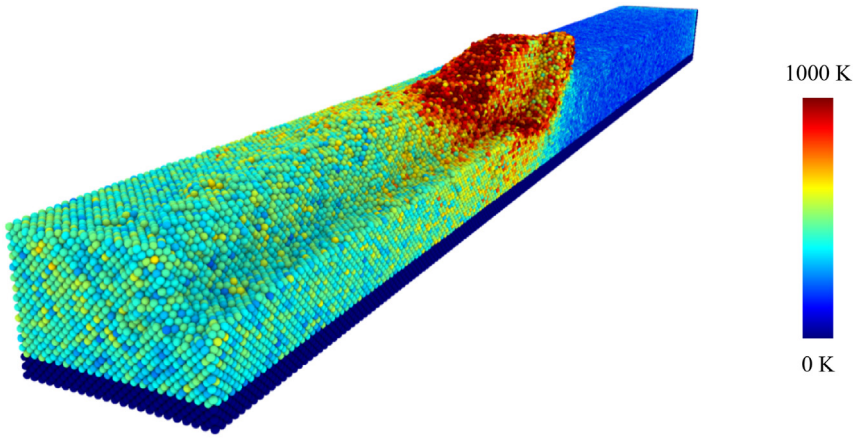


**Fig. 21.** Workpiece temperature for $v_g$ = 300 m/s and $k_g$ = 0.00125 nN/Å.

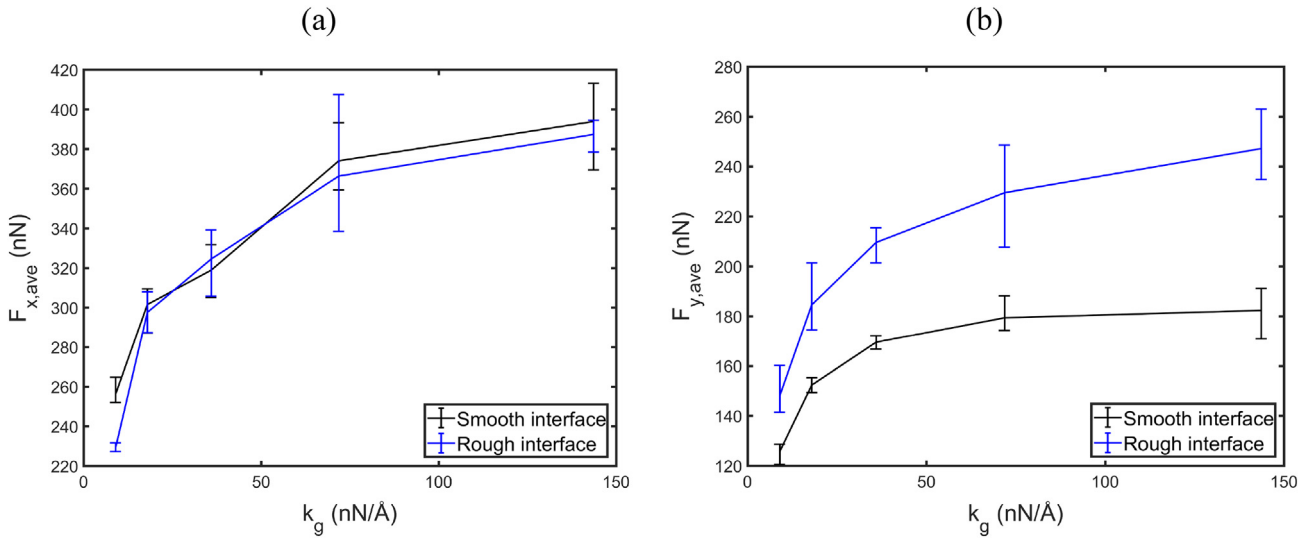


**Fig. 22.** (a) Tangential and (b) normal forces vs spring constant for different interface types.

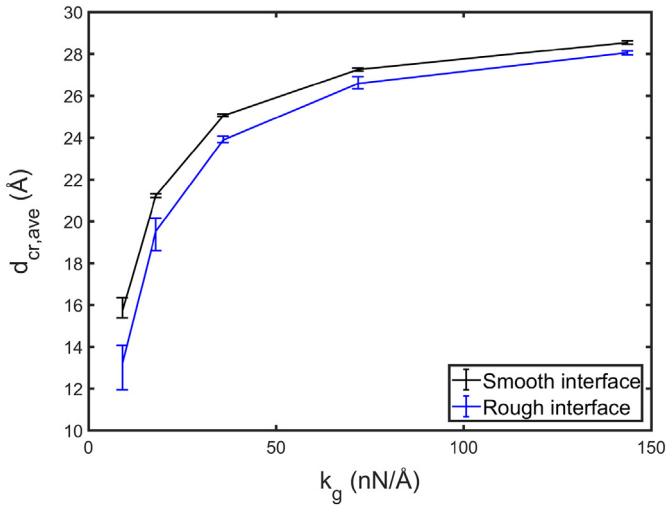


**Fig. 23.** Average real depth of cut vs spring constant for different interface types.

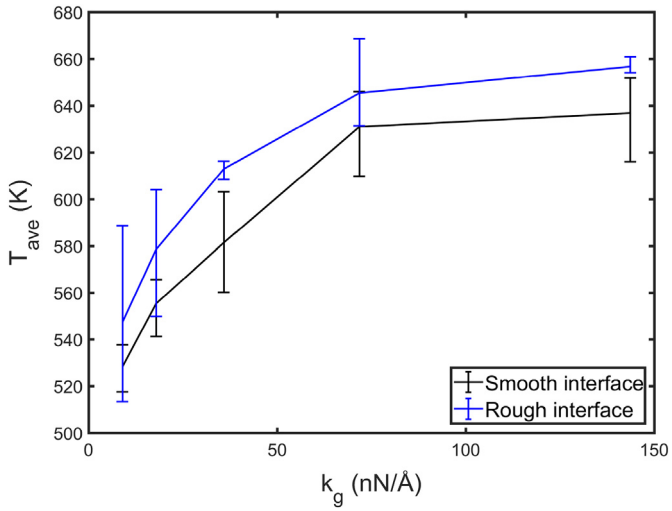


**Fig. 24.** Subsurface temperature vs spring constant for different interface types.

deviation (STD) of the y coordinate of the centre of mass of the grain was estimated. STD values are indicative of the oscillations transmitted to the abrasive grain during grinding. High STD values imply irregular ground surfaces while low values imply smooth surfaces. Fig. 19 illustrates the dependence of the STD on the grain stiffness for various grinding speeds. As shown, in all cases STD decreases for higher grain stiffness; the stiffer the grain the smoother the ground surface.

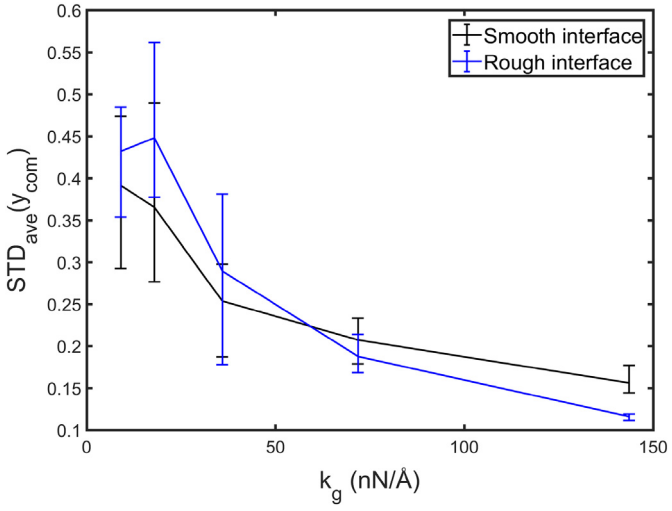


**Fig. 25.** Average STD of the y-coordinate of the centre of mass vs spring constant for different interface types.

However, Fig. 19 reveals an interesting trend as far as grinding speeds are considered. For low $k_g$ values, STD is higher for higher grinding speeds. This is because of the increased momentum transfer due to the intense collisions between the grain and workpiece atoms. However, this trend seems to be inverted as $k_g$ increases, i.e. STD decreases with the grinding speed. This is because for higher $k_g$ the subsurface temperature increases, as it will be shown in the following paragraph. Increased subsurface temperature leads to a smoother interface (higher effective viscosity) and thus, the momentum transfer between the two solids is reduced.

A summary of the effect of the grinding speed as well as the grain stiffness on the subsurface temperature is illustrated in Fig. 20. The temperature was evaluated by averaging the individual temperature of the atoms lying in the vicinity of the abrasive grain as described in Section 3.1. It is evident that subsurface temperature increases with both grain stiffness and grinding speed, as expected.

Fig. 21 shows the 3 dimensional temperature profile of the workpiece corresponding to a grinding speed, equal to 300 m/s. By comparing Fig. 21 and Fig. 14(a), it is clear that higher grinding velocities lead to higher temperatures across the workpiece. Moreover, the workpiece temperature appears to be higher compared to Fig. 14(b) which corresponds to the stiffest grain; this is in accordance to the results presented in Fig. 20. The hottest spot is located at the vicinity of the abrasive grain. The temperature of each atom was estimated according to eq. (5) and was averaged over a window of 2000 timesteps to eliminate noise.

### 3.3. Rough interface

In this section the mutual interaction of grain stiffness and rough abrasive-workpiece interface will be discussed. To introduce such an interface to the existing setup, the bottom face of the abrasive was modelled as a rough surface as illustrated in Fig. 5. As elaborated in the Introduction section, 3 different rough surface profiles with identical W-M function parameters but different random phase Φ were generated. For each one of the 5 grain stiffness values, 3 different MD experiments corresponding to the generated rough profiles were performed in order to improve statistical accuracy. The grinding speed was set equal to $v_g$ = 100 m/s and the results corresponding to the rough and smooth interface cases respectively were compared. Fig. 22(a) illustrates the effects of the interface roughness on $F_x$ as a function of the grain stiffness. It can be observed that the introduction of the rough interface does not significantly affect $F_x$ with the exception of the minimum and maximum $k_g$ values. Normally, somebody would expect lower values of $F_x$ when roughness is present due to the stronger interlocking mechanism induced [12,48]. In the following paragraphs the observed behaviour is going to be interpreted.

In contrast to $F_x$, $F_y$ values appear to be always higher when the abrasive-workpiece interface is rough (Fig. 22(b)). This is due the increased number of collisions as result of the rough interface condition which forces the abrasive to diverge from its equilibrium point in the normal axis (real depth of cut $d_{cr}$) as illustrated in Fig. 23; the higher the divergence from the equilibrium point ($d_{cr}$ = 30 Å) the higher the values of $F_y$ due to the compression of the springs attached to the abrasive grain atoms. It is clear that the difference in the real depth of cut between the two interface conditions drops for higher values of the grain stiffness. This is attributed to the increasing difference in $F_y$ between the two cases for higher grain stiffness values (Fig. 22(b)). The fact that $F_x$ remains approximately constant when the abrasive-workpiece interface is rough (Fig. 22(a)) can be explained based on the observation that the depth of cut is always lower when the interface between the two solids is irregular.

In Fig. 24, the effect of the abrasive-workpiece interface on the temperature of the workpiece in the vicinity of the tool is illustrated. It can be observed that the workpiece temperature is always higher when the interface between the two solids is rough. This is in accordance with previous MD investigations [12] and is attributed to the higher grinding forces when the interface between the two solids is rough. Besides the lower depth of cut, the increased temperature values observed in the rough interface case is an additional reason for not observing significant differences between the $F_x$ values for the two interface cases examined (Fig. 22(a)). Increased subsurface temperature contributes to the thermal softening phenomenon; consequently, the resistance imposed on the longitudinal motion (x-direction) of the abrasive is reduced. This phenomenon is intensified for stiffer grains which induce higher subsurface temperature; for this particular reason lower $F_x$ is observed for stiffer grains when the interface between the two solids is rough.

As illustrated in Fig. 25 the standard deviation of the y-coordinate of the grain centre of mass is higher when the interface is smooth and the grain stiffness low, as a result of the increased number of collisions. However, this trend is inversed for higher values of the grain stiffness; rough interfaces lead to the reduction of the vibrations transmitted from the workpiece to stiff grains. This is as well attributed to the gradual intensification of the thermal softening phenomenon as discussed in the previous section.

## 4. Conclusions

Grinding wheels are made of abrasive grits bonded together with a binder. As a result, during the grinding process, grits get deflected from the initial position due to the compression of the binder and exhibit elastic behaviour. The objective of this investigation is to investigate the contact stiffness effects on the grinding process characteristics via 3 dimensional MD simulations. The current analysis has also been expanded to the mutual interaction of grain stiffness along with grinding speed and fractal interface between the abrasive and the workpiece. MD simulations have been repeated in favour of statistical accuracy since grinding is a highly stochastic process. The yielded results are in agreement with the findings of previous numerical and experimental investigations and shed light on the interaction of a single abrasive grain with the workpiece, with respect to the grinding forces, friction coefficient, real depth of cut and subsurface temperature. The developed MD model has been proven to be capable of capturing the thermal softening phenomenon at the abrasive-workpiece interface, as reported by previous experimental studies. The most significant conclusions of this investigation are summarised below:

- The workpiece subsurface temperature increases with grinding speed and grain spring constant. Rough abrasive-workpiece interfaces lead to higher subsurface temperature as well.

- Both tangential and normal forces increase for higher grain stiffness due to the higher cutting depth induced.
- Tangential forces reduce asymptotically with the grinding speed. This is attributed to the higher subsurface temperature which contributes to the thermal softening of the workpiece.
- Tangential forces are affected by the presence of roughness according to the superposition of three phenomena (a) strong interlocking mechanism, (b) thermal softening and (c) lower depth of cut.
- Normal forces increase with the grinding speed and the presence of interfacial roughness due to the increase of the springback force with the strain rate [19]. However, for high grinding speeds normal forces appear to decrease when the grain stiffness constant exceeds a threshold.
- The friction coefficient appears to increase non-monotonically with the grain stiffness. However, it has been clear that it reduces for higher grinding speeds. This observation is in accordance with the experimentally observed viscoplastic behaviour of materials and justifies the degradation of the cutting forces with the grinding speed.
- The analysis of the standard deviation of the y coordinate of the abrasive centre of mass showed that, when the grain spring constant is over a threshold, ($\approx$50 nN/Å) high grinding speeds should be selected to obtain smoother ground surfaces. On the contrary, when the spring constant is below this threshold low grinding speeds should be selected instead.
- Rough interfaces were found to increase the standard deviation of the abrasive centre of mass for lower values of the grain stiffness and reduce it for stiffer grains.

## References


[1] E. Brinksmeier, J. Aurich, E. Govekar, C. Heinzel, H.-W. Hoffmeister, F. Klocke, J. Peters, R. Rentsch, D. Stephenson, E. Uhlmann, K. Weinert, M. Wittmann, Advances in modeling and simulation of grinding processes, CIRP Ann. Technol. 55 (2006) 667–696.

[2] L. Verlet, Computer" experiments" on classical fluids. I. Thermodynamical properties of Lennard-Jones molecules, Phys. Rev. 159 (1967) 98.

[3] L.A. Girifalco, V.G. Weizer, Application of the Morse potential function to cubic metals, Phys. Rev. 114 (1959) 687.

[4] R. Komanduri, N. Chandrasekaran, L.M. Raff, Effect of tool geometry in nanometric cutting: a molecular dynamics simulation approach, Wear 219 (1998) 84–97, https://doi.org/10.1016/S0043-1648(98)00229-4.

[5] B. Lin, S.Y. Yu, S.X. Wang, An experimental study on molecular dynamics simulation in nanometer grinding, J. Mater. Process. Technol. 138 (2003) 484–488, https://doi.org/10.1016/S0924-0136(03)00124-9.

[6] R. Komanduri, N. Chandrasekaran, L.M. Raff, Some aspects of machining with negative-rake tools simulating grinding: a molecular dynamics simulation approach, Philos. Mag. B 79 (1999) 955–968.

[7] M.S. Daw, M.I. Baskes, Embedded-atom method: derivation and application to impurities, surfaces, and other defects in metals, Phys. Rev. B 29 (1984) 6443.

[8] Q.X. Pei, C. Lu, F.Z. Fang, H. Wu, Nanometric cutting of copper: a molecular dynamics study, Comput. Mater. Sci. 37 (2006) 434–441.

[9] J. Li, Q. Fang, Y. Liu, L. Zhang, A molecular dynamics investigation into the mechanisms of subsurface damage and material removal of monocrystalline copper subjected to nanoscale high speed grinding, Appl. Surf. Sci. 303 (2014) 331–343.

[10] J. Li, Q. Fang, L. Zhang, Y. Liu, Subsurface damage mechanism of high speed grinding process in single crystal silicon revealed by atomistic simulations, Appl. Surf. Sci. 324 (2015) 464–474.

[11] S. Eder, U. Cihak-Bayr, A. Pauschitz, Nanotribological simulations of multi-grit polishing and grinding, Wear. 340–341 (2015) 25–30, https://doi.org/10.1016/J.WEAR.2015.03.006.

[12] M. Papanikolaou, K. Salonitis, Fractal roughness effects on nanoscale grinding, Appl. Surf. Sci. 467–468 (2019) 309–319, https://doi.org/10.1016/J.APSUSC.2018.10.144.

[13] J. Li, Q. Fang, L. Zhang, Y. Liu, The effect of rough surface on nanoscale high speed grinding by a molecular dynamics simulation, Comput. Mater. Sci. 98 (2015) 252–262, https://doi.org/10.1016/J.COMMATSCI.2014.10.069.

[14] T.-H. Fang, C.-I. Weng, Three-dimensional molecular dynamics analysis of processing using a pin tool on the atomic scale, Nanotechnology 11 (2000) 148–153, https://doi.org/10.1088/0957-4484/11/3/302.

[15] M. Papanikolaou, M. Frank, D. Drikakis, Nanoflow over a fractal surface, Phys. Fluids 28 (2016), https://doi.org/10.1063/1.4958975.

[16] R.S. Hahn, Effect of wheel-work conformity in precision grinding, Trans. ASME. 77 (1955) 1325.

[17] H. Li, T. Yu, L. Zhu, W. Wang, Analysis of loads on grinding wheel binder in grinding process: insights from discontinuum-hypothesis-based grinding simulation, Int. J. Adv. Manuf. Technol. 78 (2015) 1943–1960, https://doi.org/10.1007/s00170-014-6767-6.

[18] J.L. Osa, J.A. Sánchez, N. Ortega, I. Iordanoff, J.L. Charles, Discrete-element modelling of the grinding contact length combining the wheel-body structure and the surface-topography models, Int. J. Mach. Tools Manuf. 110 (2016) 43–54, https://doi.org/10.1016/J.IJMACHTOOLS.2016.07.004.

[19] G.R. Johnson, W.H. Cook, A constitutive model and data for materials subjected to large strains, high strain rates, and high temperatures, Proc. 7th Inf. Sympo. Ballist, 1983, pp. 541–547.

[20] D.M. Heyes, J. Baxter, U. Tüzün, R.S. Qin, Discrete–element method simulations: from micro to macro scales, Philos. Trans. R. Soc. London. Ser. A Math. Phys. Eng. Sci. 362 (2004) 1853–1865, https://doi.org/10.1098/rsta.2004.1420.

[21] Y. Liu, B. Li, L. Kong, A molecular dynamics investigation into nanoscale scratching mechanism of polycrystalline silicon carbide, Comput. Mater. Sci. 148 (2018) 76–86, https://doi.org/10.1016/J.COMMATSCI.2018.02.038.

[22] S. Goel, X. Luo, A. Agrawal, R.L. Reuben, Diamond machining of silicon: a review of advances in molecular dynamics simulation, Int. J. Mach. Tools Manuf. 88 (2015) 131–164, https://doi.org/10.1016/J.IJMACHTOOLS.2014.09.013.

[23] J. Shimizu, L. Zhou, H. Eda, Molecular dynamics simulation of effect of grinding wheel stiffness on nanogrinding process, Int. J. Abras. Technol. 1 (2008) 316–326.

[24] J. Shimizu, Molecular dynamics simulation of nano grinding-influence of tool stiffness, Int. J. Manuf. Sci. Technol. 9 (2007) 69.

[25] X. Guo, Q. Li, T. Liu, C. Zhai, R. Kang, Z. Jin, Molecular dynamics study on the thickness of damage layer in multiple grinding of monocrystalline silicon, Mater. Sci. Semicond. Process. 51 (2016) 15–19, https://doi.org/10.1016/J.MSSP.2016.04.013.

[26] T. Schneider, E. Stoll, Molecular-dynamics study of a three-dimensional one-component model for distortive phase transitions, Phys. Rev. B 17 (1978) 1302–1322, https://doi.org/10.1103/PhysRevB.17.1302.

[27] J. Li, Q. Fang, Y. Liu, L. Zhang, Scratching of copper with rough surfaces conducted by diamond tip simulated using molecular dynamics, Int. J. Adv. Manuf. Technol. 77 (2015) 1057–1070, https://doi.org/10.1007/s00170-014-6536-6.

[28] J.A. Harrison, J.D. Schall, S. Maskey, P.T. Mikulski, M.T. Knippenberg, B.H. Morrow, Review of force fields and intermolecular potentials used in atomistic computational materials research, Appl. Phys. Rev. 5 (2018) 031104, , https://doi.org/10.1063/1.5020808.

[29] J. Tersoff, Empirical interatomic potential for carbon, with applications to amorphous carbon, Phys. Rev. Lett. 61 (1988) 2879–2882, https://doi.org/10.1103/PhysRevLett.61.2879.

[30] D. Conrad, K. Scheerschmidt, Empirical bond-order potential for semiconductors, Phys. Rev. B 58 (1998) 4538–4542, https://doi.org/10.1103/PhysRevB.58.4538.

[31] P.M. Morse, Diatomic molecules according to the wave mechanics. II. Vibrational levels, Phys. Rev. 34 (1929) 57–64, https://doi.org/10.1103/PhysRev.34.57.

[32] L. Zhang, H. Tanaka, Towards a deeper understanding of wear and friction on the atomic scale—a molecular dynamics analysis, Wear 211 (1997) 44–53, https://doi.org/10.1016/S0043-1648(97)00073-2.

[33] N. Asproulis, D. Drikakis, Surface roughness effects in micro and nanofluidic devices, J. Comput. Theor. Nanosci. 7 (2010) 1825–1830 http://www.ingentaconnect.com/content/asp/jctn/2010/00000007/00000009/art00020 (accessed October 20, 2016).

[34] N.V.N. Priezjev, S.S.M. Troian, Influence of periodic wall roughness on the slip behaviour at liquid/solid interfaces: molecular-scale simulations versus continuum predictions, J. Fluid Mech. 554 (2006) 25–46 http://journals.cambridge.org/abstract_S0022112006009086 (accessed November 8, 2016).

[35] B.B.-Y. Cao, M. Chen, Z.Z.-Y. Guo, Effect of surface roughness on gas flow in microchannels by molecular dynamics simulation, Int. J. Eng. Sci. 44 (2006) 927–937 http://www.sciencedirect.com/science/article/pii/S0020722506001042 (accessed January 20, 2016).

[36] C.K. Bora, E.E. Flater, M.D. Street, J.M. Redmond, M.J. Starr, R.W. Carpick, M.E. Plesha, Multiscale roughness and modeling of MEMS interfaces, Tribol. Lett. 19 (2005) 37–48, https://doi.org/10.1007/s11249-005-4263-8.

[37] A. Majumdar, B. Bhushan, Role of fractal geometry in roughness characterization and contact mechanics of surfaces, ASME J. Tribol. 112 (2) (1990) 205–216 http://tribology.asmedigitalcollection.asme.org/pdfaccess.ashx?ResourceID=4636202&PDFSource=13 , Accessed date: 5 March 2016.

[38] M. Ausloos, D.H. Berman, A multivariate Weierstrass-Mandelbrot function, Proc. R. Soc. Lond. A Math. Phys. Sci. 400 (1985) 331–350 http://rspa.royalsocietypublishing.org/content/400/1819/331.short , Accessed date: 7 March 2016.

[39] S. Plimpton, Fast parallel algorithms for short-range molecular dynamics, J. Comput. Phys. 117 (1995) 1–19.

[40] LAMMPS Molecular Dynamics Simulator, (n.d.). https://lammps.sandia.gov/.

[41] J. Li, Q. Fang, Y. Liu, L. Zhang, A molecular dynamics investigation into the mechanisms of subsurface damage and material removal of monocrystalline copper subjected to nanoscale high speed grinding, Appl. Surf. Sci. 303 (2014) 331–343, https://doi.org/10.1016/J.APSUSC.2014.02.178.

[42] K. Salonitis, T. Chondros, G. Chryssolouris, Grinding wheel effect in the grind-hardening process, Int. J. Adv. Manuf. Technol. 38 (2008) 48–58, https://doi.org/10.1007/s00170-007-1078-9.

[43] D. Anderson, A. Warkentin, R. Bauer, Experimental and numerical investigations of single abrasive-grain cutting, Int. J. Mach. Tools Manuf. 51 (2011) 898–910.

[44] R.L. Johnson, M.A. Swikert, E.E. Bisson, Friction at High Sliding Velocities, https://digital.library.unt.edu/ark:/67531/metadc55542/, (1947) , Accessed date: 19 February 2019.

[45] Y. Sang, M. Dubé, M. Grant, Dependence of friction on roughness, velocity, and

temperature, Phys. Rev. E 77 (2008) 036123, , https://doi.org/10.1103/PhysRevE.77.036123.
[46] J. Li, Q. Fang, L. Zhang, Y. Liu, The effect of rough surface on nanoscale high speed grinding by a molecular dynamics simulation, Comput. Mater. Sci. 98 (2015) 252–262, https://doi.org/10.1016/J.COMMATSCI.2014.10.069.
[47] J. Shimizu, L.. Zhou, H. Eda, Simulation and experimental analysis of super high-speed grinding of ductile material, J. Mater. Process. Technol. 129 (2002) 19–24, https://doi.org/10.1016/S0924-0136(02)00568-X.
[48] O.K. Panagouli, K. Iordanidou, Dependence of friction coefficient on the resolution and fractal dimension of metallic fracture surfaces, Int. J. Solids Struct. 50 (2013) 3106–3118, https://doi.org/10.1016/J.IJSOLSTR.2013.05.020.

2019-07-04

# Contact stiffness effects on nanoscale high-speed grinding: A molecular dynamics approach

Papanikolaou, Michail

Elsevier

Papanikolaou M, Salonitis K. Contact stiffness effects on nanoscale high-speed grinding: A molecular dynamics approach. Applied Surface Science, Volume 493, 1 November 2019, pp. 212-224
https://doi.org/10.1016/j.apsusc.2019.07.022